MIT Libraries | DSpace@MIT

MIT Open Access Articles

Grain boundary and triple junction constraints during martensitic transformation in shape memory alloys

Massachusetts Institute of Technology

Grain boundary and triple junction constraints during martensitic transformation in shape memory alloys

Stian M. Ueland and Christopher A. Schuh

Additional information on J. Appl. Phys.

Grain boundary and triple junction constraints during martensitic transformation in shape memory alloys

Stian M. Ueland and Christopher A. Schuh[a)]
Department of Materials Science and Engineering, Massachusetts Institute of Technology,
77 Massachusetts Avenue, Cambridge, Massachusetts 02139, USA

We investigate the role of grain constraint upon martensitic transformation through *in situ* scanning electron microscope tensile experiments on shape memory microwires with a small number of grains and grain junctions. The martensite transformation morphology becomes more complex with increasing grain constraint: In unconstrained monocrystalline regions, the transformation is simple, single variant, and complete; near grain boundaries, the transformation is only partial, containing regions of untransformed austenite; near a triple junction, the morphology is complex, the transformation is partial and also multi-variant. These observations speak of transformation-induced stress concentrations that are more severe around triple junctions than around grain boundaries. Finite element modeling also provides an estimate for constraint effects on martensitic transformation yielding higher stresses near triple junctions than near grain boundaries. Towards the goal of developing polycrystalline Cu-based shape memory alloys that avoid intergranular fracture, our results support three design objectives: (1) Removal of triple junctions, (2) reduction of the total grain boundary area, and (3) geometry design containing unconstrained regions where the transformation can be most easily accommodated. © *2013 AIP Publishing LLC*.
[http://dx.doi.org/10.1063/1.4817170]

I. INTRODUCTION

Shape memory alloys (SMAs) are characterized by a reversible phase transformation from the higher symmetry austenite to the lower symmetry martensite.[1–3] The transformation is sensitive to material microstructure, such as grain orientation,[4,5] grain size,[6–8] and grain boundary character.[9] For example, by varying only sample orientation, the reversible superelastic strain in single crystals can vary between 4% and 8.3% in Cu-Al-Ni.[4] Furthermore, fracture of SMA bicrystals can be intergranular or transgranular depending on crystallographic misorientation.[10] Finally, both the size and shape of superelastic stress strain curves change with grain size.[11]

While microstructure is important in all SMAs, the large anisotropy of their transformation strains renders the Cu-based alloys particularly sensitive and leads to widely different behavior in single crystals and polycrystals.[12] In fact, while single crystals show excellent SMA properties, their polycrystalline counterparts perform very poorly and often suffer from intergranular fracture.[10,13–17] When designed with a bamboo grain structure, however, Cu-Zn-Al and Cu-Al-Ni wires show shape memory, superelastic, and fatigue properties that approach those of single crystals.[18] The excellent performance of these "oligocrystalline" shape memory alloys (oSMAs) has been attributed to the reduced grain boundary area, the removal of triple junctions, and stress relaxation at free surfaces.[18–20] So far, however, the studies on such structures are purely thermomechanical, and these

explanations remain in need of more quantitative evaluation and comparison.

In addition to altering mechanical properties, material microstructure also affects martensite transformation morphology.[21–26] The many *in situ* studies on stress-induced martensite, both with transmission electron microscopy (TEM) and optical microscopy (OM), speak of a relatively simple transformation path in single crystals.[1,27–30] For example, *in situ* OM of Cu-Al-Ni shows complete single variant transformation in single crystals.[27] The few studies on polycrystals, on the other hand, speak of very complicated morphologies and stress fields.[28,31] For example, in Cu-Zn-Al and Ni-Ti, a myriad of small plates of different variants can be found within a single grain and variants in adjacent grains can couple.[27,28] Furthermore, the amount of martensite that is observed to form is limited by "locking" of the variant structure as sequential grain transformation occurs.[28] The large gap in complexity between these two extremes renders interpretation of the individual role of crystal, near-grain boundary, and near-triple junction regions difficult.

On the computational side, numerical simulations of SMAs have mostly been directed towards the development of "macroscopic" constitutive models based on thermodynamics.[32–39] The impact of grain boundaries on stress fields as well as coupling between grains has been studied less frequently[36,40,41] and transformation-induced fracture has not been addressed. For non-SMA materials, on the other hand, the finite element methods as well as other numerical techniques has been used to investigate intergranular stresses, incorporating, for example, anisotropic elastic or plastic material behavior.[42–48]

In this paper, we use oSMA wires to investigate the morphology of stress-induced martensite as the degree of

---

a)Author to whom correspondence should be addressed. Email address: schuh@mit.edu

microstructural complexity is increased. We first present *in situ* tensile explorations of the stress-induced superelastic transformation, beginning with a single crystalline region, then proceeding to examine a region near a grain boundary, and finally, a region near a triple junction. The level of increasing constraint is apparent in the complexity of the transformation kinematics in such structures. To provide context for the experimental observations, we also use a simple anisotropic finite element model to estimate the constraint effects on martensitic transformation near grain boundaries and triple junctions in such wires. The results provide support for the further development of oligocrystalline SMAs, and some guidelines for their microstructure.

II. MATERIALS AND EXPERIMENTAL METHODS

The wires presented here were prepared by placing solid pieces of shape memory alloy inside a closed-end aluminosilicate glass tube. The metal composition was Cu–22.9% Zn–6.3% Al (wt. %), the glass inner diameter was 4 mm, and the glass working temperature was ∼1250 °C. The inside of the glass tube was then subjected to low vacuum conditions and an oxy-acetylene burner was used to melt the metal inside the tube. The heating also softened the glass, which was then manually drawn out of the hot zone with the molten metal at its core. By varying the drawing speed, we were able to obtain glass coated metallic filaments of different diameters, ranging from ∼20 to a few hundred μm.

To promote grain growth into the stable bamboo structure, the glass-coated wires were annealed in an argon atmosphere for 3 h at 800 °C and water quenched. The glass coating was then chemically etched away by immersion in ∼10% diluted aqueous hydrofluoric acid. The wires were electropolished in an electrolyte consisting of 67% phosphoric acid and 33% deionized water for 30–120 s depending on wire size. The electrolyte was stirred at 80 rpm, the electrodes were pure Cu, and the polishing voltage was 2.8 V.

Transformation temperatures were found by differential scanning calorimetry (using a Discovery DSC from TA instruments) at a scan rate of 10 °C·min^{-1}: $A_f \sim 25$, $A_s \sim 9$, $M_s \sim 8$, and $M_f \sim -6$ °C (austenite finish and start, and martensite start and finish, respectively). To determine texture and grain aspect ratio, electron backscatter diffraction (using a FEI Helios Nanolab 600 SEM equipped with a HKL CHANNEL 5 EBSD system and a Nordlys detector) was performed on the surface of polished wires. At room temperature, the material is austenitic and the diffraction bands were therefore matched to a reference B2 unit cell found in an alloy of similar composition.[49]

The *in situ* superelastic loading experiments were performed at room temperature using a deformation stage (Gatan Microtest 200) inside of a scanning electron microscope (JSM-6610LV SEM). The computer-controlled stage was operated in deformation mode and epoxy was used at the wire ends to ensure wire straightness and sound mechanical contact with the grips. All wires were tested in pure tension. The wire surface was monitored *in situ* during the test and deformation was interrupted at regular intervals to obtain high quality images as the wire transformed. The strain rate was ∼10^{-4} s^{-1}; no "dynamic" effects, such as variant redistribution, were observed between deformation interruption and image capturing. The reported strains represent "local" values inferred from the images; they were measured between grain boundaries or features on the wire surface. If not specifically mentioned, images are from wires that have undergone 1–5 previous transformation cycles. The gauge lengths for different wires were between 10 and 15 mm. The imaged regions constituted 1%–4% of the full gauge length.

III. TEXTURE AND GRAIN ASPECT RATIO

The microstructure of the wires presented here is generally one of a string of grains that meet at grain boundaries roughly perpendicular to the wire axis, i.e., a bamboo microstructure. In Fig. 1(a), we show an image of a wire with such microstructure, with diameter D and grain length along the wire axis, d. Fig. 1(b) shows inverse pole figures (IPF) of two different wires (the left and right IPFs are from wires with diameters of 48 and 70 μm, respectively). Each point represents the orientation of an individual grain in the wire

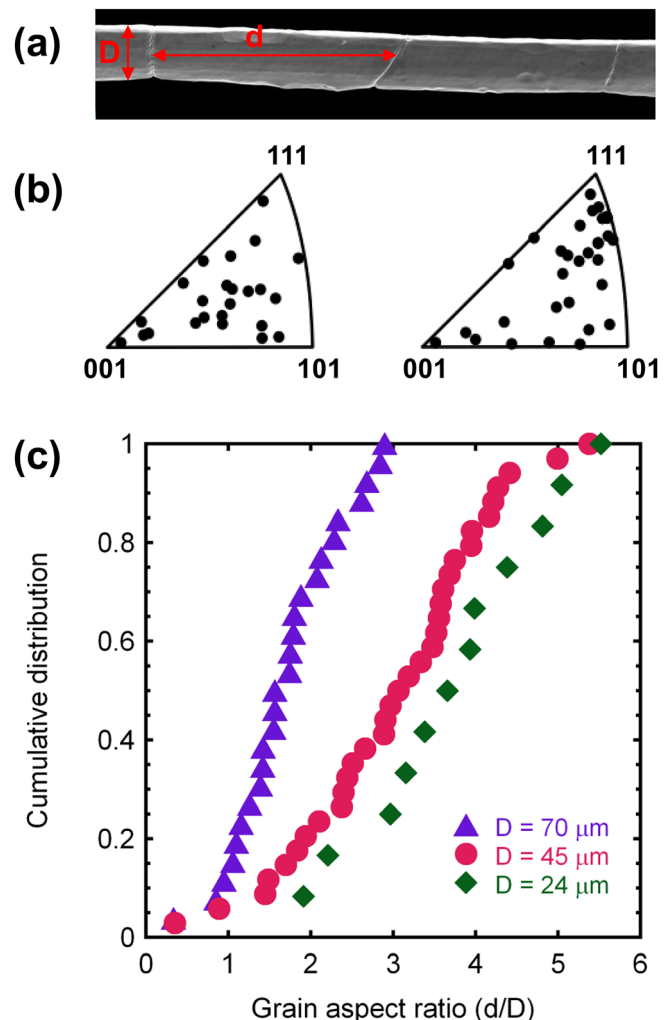FIG. 1. (a) Scanning electron micrograph of wire with bamboo grain structure showing characteristic lengths, d and D. (b) Inverse pole figures of two wires where each pole represents crystal orientation along the wire axis for a particular grain (the left and right IPFs are from wires with diameters of 48 and 70 μm, respectively). (c) Cumulative distributions of grain aspect ratios for three wires.

axis direction. The poles do not appear to exhibit any particularly strong texture, although it should be noted that the sampling statistics are very limited here due to the large size of the grains and the one-dimensional nature of the grain structure.

The cumulative distribution of grain aspect ratios, d/D, is shown for three different wires in Fig. 1(c). The average aspect ratios are 3.7, 3, and 1.7 for the wires with diameters 24, 45, and 70 μm, respectively. The number of data points is limited but there appears to be a trend towards larger aspect ratios in smaller wires. The average values are close to both experimental and simulated values in other annealed fine structures.[50] For example, simulations by Walton *et al.* yielded a grain aspect ratio of 2.3 in thin-film strips[51] and annealed Cu-Al-Mn wires with a diameter of 0.48 mm showed an average aspect ratio of up to 4.9.[8]

IV. *IN SITU* OBSERVATIONS OF MARTENSITE MORPHOLOGY

A. Morphology of stress-induced martensite in a single grain

Fig. 2 shows a previously uncycled wire with a diameter of 32 μm and a typical bamboo grain structure: the grains have aspect ratios larger than one and span the wire axis. In this and subsequent figures, we have enhanced the contrast of the martensite phase for visual clarity; raw images are made available as supplemental material online.[52] As the wire is stretched, a martensite plate is formed at the center
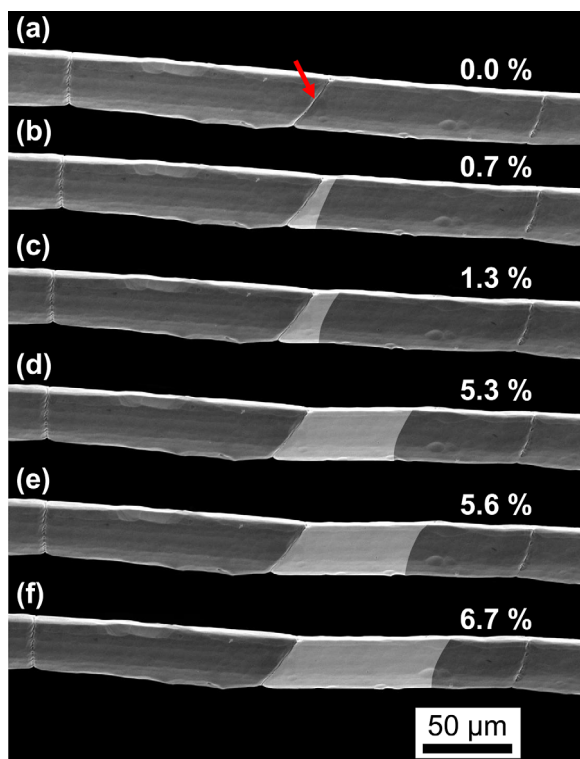

FIG. 2. Stress-induced martensite morphology during the first loading cycle of a wire with diameter 32 μm. The strain is measured between the grain boundaries of the grain undergoing transformation (the grain to the right of the grain boundary marked by a red arrow). The contrast of the martensite phase has been enhanced for visual clarity.

grain boundary (marked with a red arrow) and grows towards the right in a monolithic fashion. Because the test temperature is very close to A_f, the reverse transformation was not observed upon unloading in this case.

This wire shows many of the characteristic features of fine-scale bamboo-structure SMAs. First of all, the transformation is sequential owing to differences in grain orientation; some favorably oriented grains may fully transform while adjacent grains remain austenitic. Furthermore, the crystalline region away from grain boundaries is unconstrained and fully transforms, i.e., there is no austenite left after the interface has passed, in contrast to polycrystals where austenite only partially transforms due to the "locking" of a variant structure.[27,28] The transformation is also single-variant, again in contrast to the more complex multi-variant morphologies seen in polycrystals. A particularity of this sample, however, is the selection of a martensite variant with habit plane parallel to the center grain boundary (at least from our angle of observation). Finally, the grain boundary acts as a nucleation site and the transformation proceeds by nucleation and growth of a single martensite plate. This single-domain morphology is different from the multi-domain, more nucleation-dominated, one in large single crystalline SMAs, which we have attributed to the decreased sampling of obstacles in small samples.[53]

B. Morphology of stress-induced martensite near a grain boundary

1. Fine wire

Fig. 3 shows the evolution of martensite near a grain boundary in a wire with diameter 32 μm. The first panel (a) shows the wire before loading; in the second panel (b), two martensite plates of the same variant have nucleated simultaneously. As in Fig. 2, nucleation occurs near the grain boundary, but because the variant is inclined to the grain boundary (by $\sim 20° \pm 5°$ as measured at the wire center line), they only contact the boundary at a point on the top of the wire in the view of Fig. 3. As further deformation is imposed, the two plates (c) coalesce and eventually (d) the entire left grain is transformed, with the exception of a narrow wedge of austenite that remains adjacent to the grain boundary. After the leftward-propagating transformation has been exhausted, the phase interface near the grain boundary begins to advance to the right in panel (e). However, the wedge of untransformed austenite between the main plate and the grain boundary remains preserved in this grain even as new martensite is nucleated in the right grain in panels (d)–(f).

Several observations from the final three panels (d)–(f) of Fig. 3 are noteworthy. First, the various martensite plates in the right grain in panel (e) are inclined differently to the wire axis from one another, as shown by the marked angles "a" and "b" (note that the apparent curvature of the interfaces is a viewing parallax issue). This geometric inconsistency suggests that the corresponding martensite domains "M1" and "M2" are two different variants; the grain is likely near a symmetric orientation with the two variants having similar Schmid factors. The bending caused by martensite formation elsewhere in the wire as well as the presence of the grain boundary probably also alters the local stress state, facilitating
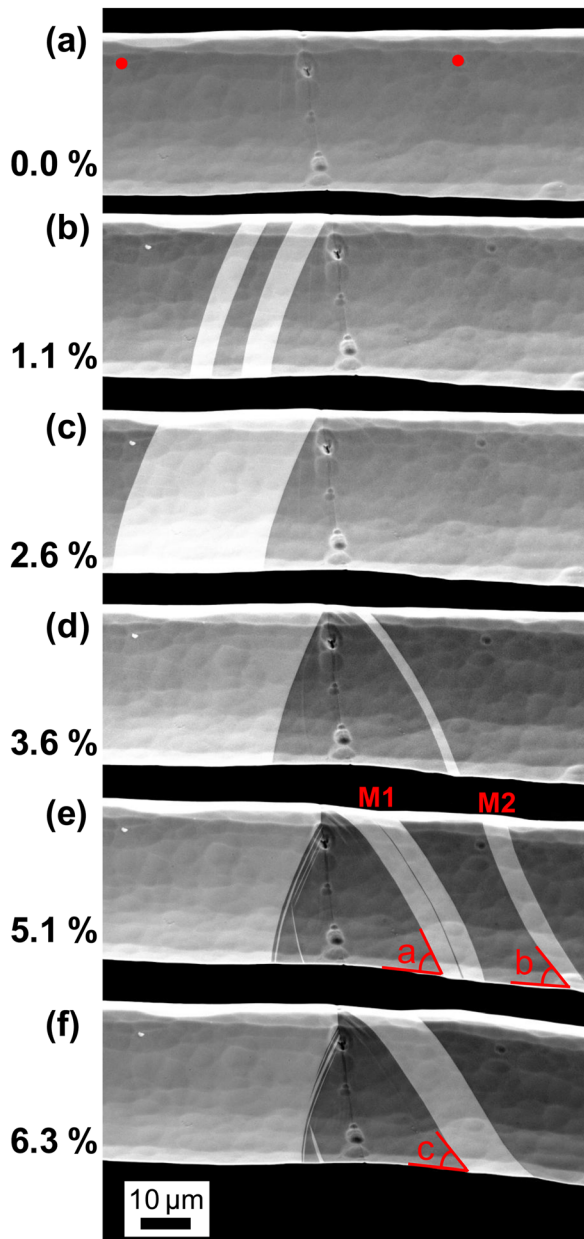
FIG. 3. Stress-induced martensite morphology near a grain boundary in a wire with a diameter of 32 μm. The local strain is measured between the points indicated by red circles in panel (a). M1 and M2 in panel (e) denote two different martensite variants in the right grain. The angles in panels ((e)–(f)) are a = 60, b = 45, and c = 45° ± 5°. The angles are local angles measured at the bottom of the wires; they do not correct for wire curvature. The contrast of the martensite phase has been enhanced for visual clarity.

a multi variant morphology. Interestingly, as the wire is further stretched from panel (e) to (f), M2 disappears, i.e., the part of the wire occupied by M2 in panel (e) transforms back to austenite, while M1 remains. However, whereas the location of the martensite plate in panel (f) is that of M1 in panel (e), the plate appears geometrically more like a hybrid of the two variants. The local angles, labeled "a" and "b" in panel (e), are measured to be 60° and 45° ± 5°, respectively, and the local angle of the martensite plate in panel (f), "c" is 45° ± 5°; these measurements do not correct for the viewing parallax issue. At the top of the wire, the local variant inclination (angle measurement not shown) is therefore similar to

that of variant M1 in panel (e), whereas at the bottom, it resembles that of variant M2.

While the structure in the right grain develops, the martensite morphology in the left grain continues to evolve. Even at the full 6.3% applied strain level, the region near the grain boundary resists transformation, which is apparently a result of grain boundary constraint upon the transformation shape change. However, as the applied strain increases, the austenite/martensite interface is pushed towards the right, and accommodation of the constraint begins to trigger additional transformation events. In panels (e) and (f), we observe small plates that do not span the cross section and some that are even oriented at a different inclination from the main plate. The observation that several variants are needed to accommodate the applied strain is direct evidence that the stress state near the grain boundary is different from the single-variant uniaxial loading condition that prevailed earlier in the test in the center of the left grain.

The observations in Fig. 3 are very different from those of the special case of Fig. 2 where the habit plane aligned with the grain boundary. Fig. 3 shows how the transformation is effectively constrained at grain boundaries: higher stresses are needed to transform and when it transforms it does so only partially. The sequence in Fig. 3 shows that it is easier for the specimen to transform in regions away from grain boundaries, so most of the early transformation strain is accommodated in grain interiors. We conclude that even though grain boundaries are present in oSMAs, stress concentrations are not allowed to build up there in the same way as they are in conventional polycrystals.

2. Coarser wire

Before we proceed to look at the transformation near a grain boundary in a large wire, a few notes concerning the image enhancement are in order. Fig. 4 shows three versions of the same image. In (a), the raw image is presented and martensite plates can be distinguished, especially in the upper part of the right grain. In (b), we have increased their contrast by carefully tracking plates from earlier images at high magnification. In the center bottom part of the wire, although martensite plates can clearly be observed at higher magnification, the contrast is too low for accurate enhancement. In (c), we have increased the contrast in that region to reflect the overall microstructure, but it should be understood that some interpretation has been introduced. In the images to follow, only plates that are clearly distinguishable from the austenite are enhanced, but it is understood that martensite also forms in the lower center region even though they are not clearly visible here. Raw images for all of the figures in this paper are included in the supplemental information for Ref. 52.

Fig. 5 shows the evolution of martensite near a grain boundary in a wire with diameter 116 μm during a full superelastic cycle. Panels (a)–(f) show the forward transformation while panels (g)–(j) show the reverse transformation. The maximum strain is reached in panel (f). Because the test temperature is very close to A_f, some residual martensite plates, which are mostly in contact with the grain boundary, are present in the right grain both before and after loading.
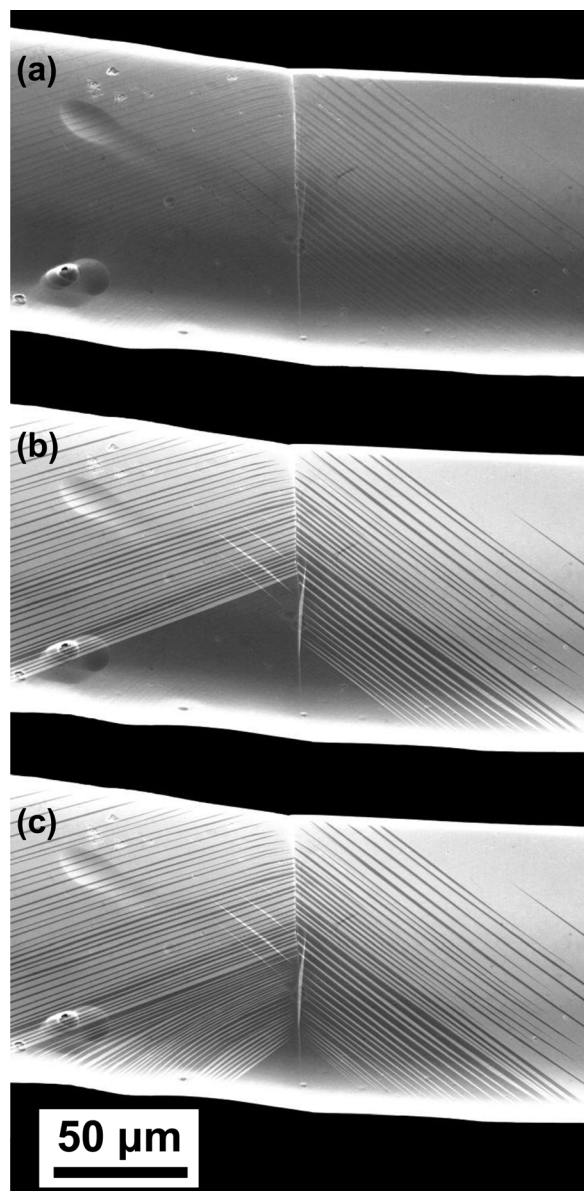
FIG. 4. Three versions of the same scanning electron micrograph. In (a), the raw image without contrast enhancement is shown. In (b), we have enhanced the contrast of the martensite plates that are clearly distinguishable, tracking them from earlier images at less strain. In (c), we have enhanced the contrast of all martensite plates, even those that are not clearly distinguishable in the lower center part of the wire.

Some aspects of the transformation in the coarse wire are similar to what was observed in the fine wire. For example, we see that one grain (the right) starts transforming before the other and also that martensite is more stable in this grain during the reverse transformation. We also see that plates form at angles of ~70 and 50° ± 5° (left and right grain, respectively) with the grain boundary plane; but after nucleation, they grow little or not at all. Plates away from the grain boundary, however, exhibit more growth. The plate angle is larger than was the case in the finer wire and the area affected by the grain boundary is therefore larger too.

There are also several morphological or kinematic differences between the fine and the coarse wire. The most striking feature of Fig. 5 is the large number of thin

individual plates that are in contact with the grain boundary. These plates nucleate, but do not grow considerably or coalesce with their neighbors. Furthermore, in panel (f), a plate (4) is formed in the right grain very close to the grain boundary and three thin plates (1)–(3) of a different variant are observed in the left grain. This phenomenon, suggesting that it is preferable to nucleate new variants that cross over the old ones instead of growing existing ones, clearly speak of the confining effect of the grain boundary on the transformation. Finally, the majority of the first plates to nucleate are contacting the grain boundary, which may reflect the ease of nucleation there. On the other hand, as in the finer wire, the grain boundary region only transforms partially and further transformation is mostly accommodated by the regions away from the boundary.

Although some of the differences between the fine and the coarse wire can be ascribed to grain orientations, the transformation seems, at least qualitatively, to be more constrained in the coarser wire. This conclusion is reasonable because there is more grain boundary area per wire length in coarser wires, even at identical grain aspect ratios.

C. Morphology of stress-induced martensite near a triple junction

The stable microstructure for annealed microwires is the bamboo structure observed in Figs. 2–5. One large wire with a diameter of 150 μm, however, contained a triple junction and the evolution of martensite during the loading part of a superelastic curve in this region is shown in Fig. 6. The tensile direction is horizontal and the triple junction joins two large bamboo-like grains (the lower left and lower right grains) and one small "island" grain (the upper center grain) that does not span the wire cross section. In panel (a), the wire is already under stress and the martensite has been induced in two of the grains. In the three successive images, the wire is further deformed and the martensite morphology evolves. The unloading part is not shown but the reverse transformation is similar to the forward one and the wire returns to austenite.

In Fig. 6, we observe a large number of martensite nucleation events followed by some growth. The growth is very limited, however, and parallel plates do not grow sufficiently to connect with their neighbors. In fact, the transformation is only partial everywhere in the field of view and larger plates (in the lower right grain) even split into smaller plates as stress is increased from (b) to (c). In panel (c) of Fig. 6, a new variant appears in the lower left grain, much like the new variants observed near the grain boundary in Fig. 5. Interestingly, many new plates of this variant are observed in (d) and these appear to grow at the expense of the first variant. A similar crossing of variants is observed in the small upper center grain near the boundary. This complex morphology is similar to what is seen in polycrystalline samples where variants are commonly observed to cross and couple.[27,28] Presumably, the first variant has the most favorable orientation relative to the tension axis. However, as stresses build up due to the incompatibility of transformation strains at the grain boundaries, the strain energy penalty of that variant becomes too large and another variant becomes more
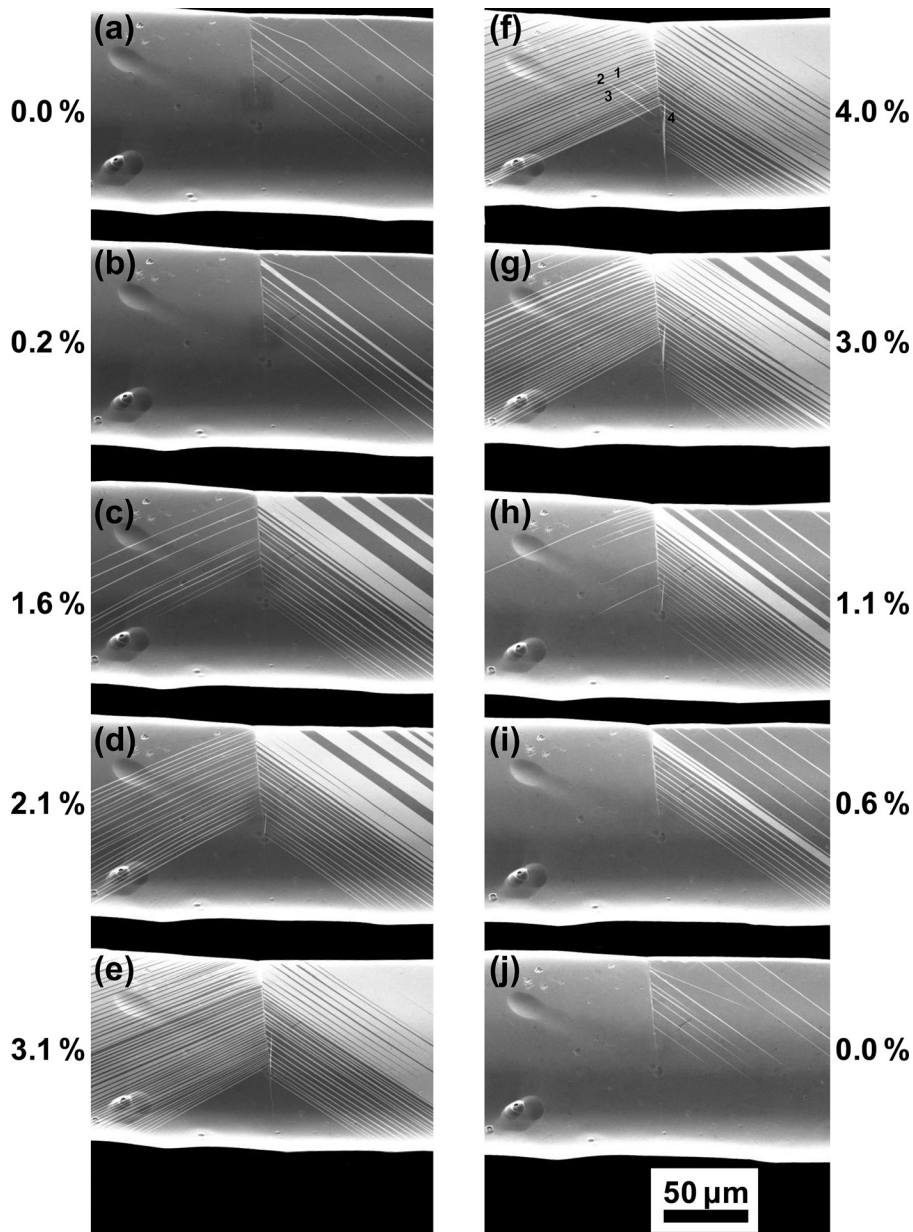
FIG. 5. Stress-induced martensite morphology near a grain boundary in a wire with a diameter of 116 μm. Panels ((a)–(f)) are from the loading whereas panels ((g)–(j)) are from unloading. The local strain is measured between the points indicated by red circles in panel (a). The numbers 1–4 in panel (f) denote particular martensite plates discussed in the text. The contrast of the martensite phase has been enhanced for visual clarity.

favorable. It is interesting to note that the first set of plates is formed to the left of the field of view and grows towards the triple junction. The second variant, on the contrary, is formed at the triple junction and grain boundaries, grows outwards and exhibits a spear-like morphology.

D. Training

Fig. 7 shows a close-up of the same wire from Fig. 2, with a magnified field-of-view focused upon the right grain from Fig. 2. The sequence of images in Fig. 7 pertains to the fifth cycle, i.e., after four straining cycles each followed by heating to recover the parent phase. The first martensite plate now appears inside the grain as opposed to at the grain boundary (cf. Fig. 2 during the first cycle). After this first plate has experienced some growth, a second plate nucleates at the left grain boundary in panel (d) as it did during the first cycle in Fig. 2. These two plates then grow simultaneously

until they coalesce. Cycling to as many as 30 cycles (not shown here) was performed and no further evolution of the transformation kinematics was observed.

Repeated stress-induced transformation is related to the formation of dislocations and arrangement of dislocation tangles.[54] The nucleation point in the interior region of the grain in Fig. 7 is therefore likely a result of a lower nucleation barrier due to the development of a dislocation substructure. In our prior work, we showed that these oSMA wires (of similar composition and diameter) exhibited a shakedown of the martensite transformation stresses during superelastic cycling, as well as the entire forward transformation plateau.[19] The hysteresis size, too, decreased by a factor of two from the first to the tenth cycle.[19] The present observations in Figs. 2 and 7 align with our prior data and provide a microstructural justification for the observed macroscopic behaviors; cycling leads to the evolution of preferred martensite nucleation sites in these oSMA wires.
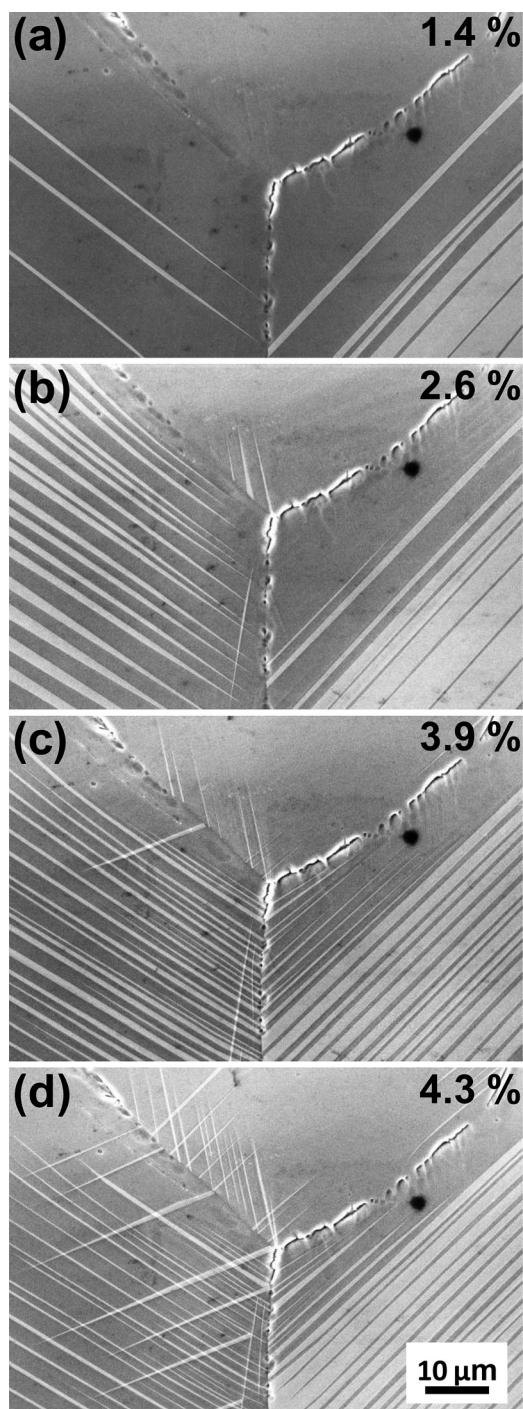
FIG. 6. Stress-induced martensite morphology near a triple junction in a wire with a diameter of 150 μm. The tensile stress is in the horizontal direction and the wire is already under stress in the first panel. The local strains indicated in the upper right corner of each panel are measured through the triple point in the tensile direction. The contrast of the martensite phase has been enhanced for visual clarity.
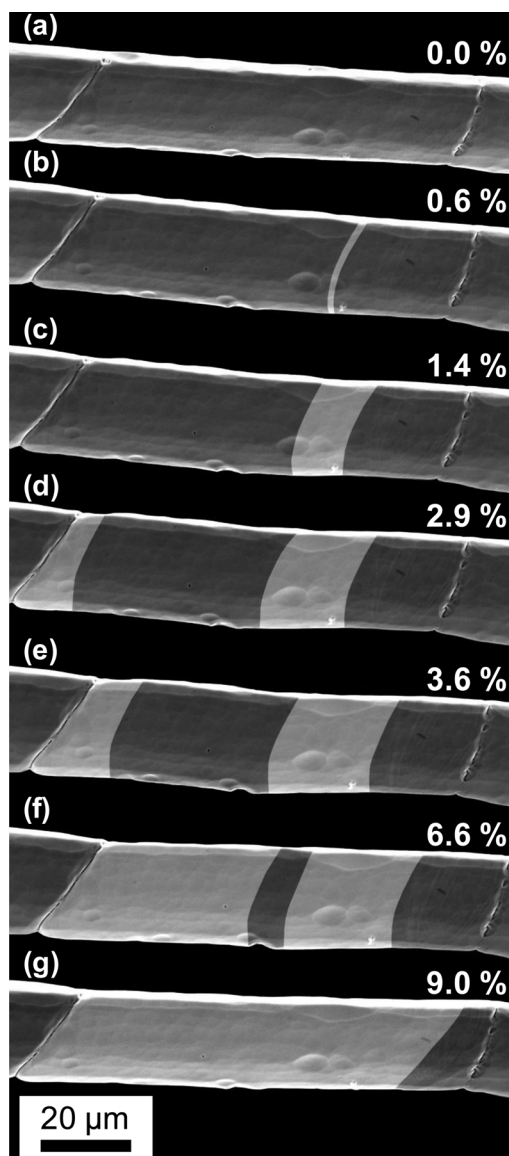

FIG. 7. Stress-induced martensite morphology in the same wire as in Fig. 2 but for the fifth superelastic cycle. The local strain is measured between the two grain boundaries. The contrast of the martensite phase has been enhanced for visual clarity.

V. CONSTRAINTS AT GRAIN BOUNDARIES AND TRIPLE JUNCTIONS

The phase morphologies observed above show that, in line with intuition, the martensitic transformation is more constrained near grain boundaries than away from them. The austenite near grain boundaries appears restricted from fully transforming and this leads to complex and even multi-variant martensite morphologies. What is more, the constraint appears to increase with increasing microstructural complexity as the triple junction replaces the grain boundary; the nucleation of a second martensite variant from grain boundaries in the vicinity of the triple junction, which grows and "crosses over" the first variant, hints of large transformation-induced stress concentrations. These observations connect to studies on polycrystals where grains are constrained at all sides, the morphology is even more complex and multi-variant and where partial transformation is commonly observed.[27,28] The complex morphology in polycrystals too has been related to local transformation-induced alterations in the stress field near grain boundaries.[28]

Because grain size determines many key SMA properties, effort has gone into understanding the role of grain constraint and particularly when it comes to fracture.[13–17,55] Although other mechanisms have been proposed, such as high elastic

anisotropy and impurity segregation, one widely held view is that intergranular fracture in SMAs is caused by the large orientation-dependence of transformation strains.[9,10,12–16] This viewpoint is supported by experimental studies demonstrating intergranular fracture upon martensitic transformations of large strain incompatibility.[13,15] The multi-variant morphology observed in this and other studies also indirectly speak of stress concentrations due to grain constraint.

In order to better understand the constraint effects on martensitic transformation near a grain boundary and a triple junction, we perform simple three-dimensional, anisotropic finite element calculations. We model Cu-Zn-Al, which transforms from a cubic austenite structure to a monoclinic martensite structure.[56] Twelve symmetrically related martensite variants and combinations of them are possible.[57] Each martensite variant is related to the austenite crystal structure by a transformation matrix, which we have included in the appendix of this article.[56] The modeled geometry is a wire with an aspect ratio of ten that is pinned at the bottom and free elsewhere. Fig. 8 shows schematics of the wire geometry, boundary conditions, and mesh geometries for both the grain boundary and the triple junction. Three-dimensional reduced-integration hexagonal elements are used.

Variant selection is made by assuming a small tensile biasing stress along the wire axis, which selects the variant that maximizes the strain along the wire axis but is negligible in the stress calculation.[58] We assign the grains random orientations, determine which variant in which grain will be induced, and assign that specific shape change to the entire top grain. Thus, we do not attempt to capture the full complexity of martensite domain formation and stress localization around domains; we simply seek to understand the "fully constrained" problem in which one grain bodily changes shape when the other(s) do not. The problem of stress distribution after the transformation is then solved as a linear anisotropic elastic problem using the commercially available finite element software ABAQUS. The mesh size was found by gradual refinement around the grain boundaries until the solution stabilized at around 20 000 elements. For these calculations, we use a material stiffness matrix[59] and martensite transformation matrices[56,60] from Cu-Zn-Al.

In Fig. 9, we show a typical result of these simulations for a wire containing a single grain boundary after the entire top grain has undergone the transformation. The images show the results as contours of tensile stress (the component along the wire axis and normal to the boundary) and von Mises stress at the wire surface and interior as well as at the wire midplane (the grain boundary plane). The focus here is on the rupture and distortional stresses because they commonly serve as failure criteria for brittle materials.[61] It can be seen that both stresses reach their maxima at the grain
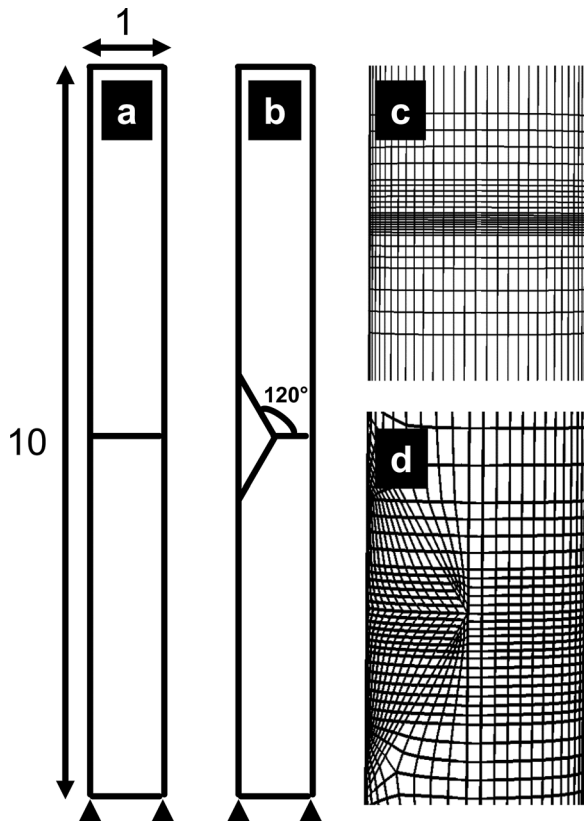

FIG. 8. Schematics showing the geometry and boundary conditions of (a) the grain boundary and (b) the triple junction. Mesh around the (c) grain boundary and (d) triple junction.
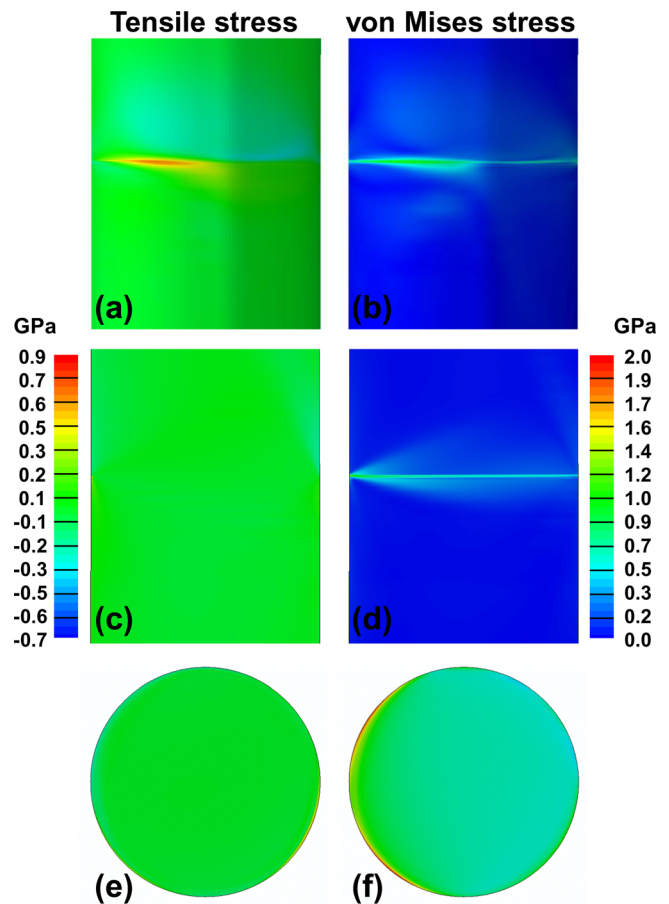

FIG. 9. Stresses near grain boundary after the upper grain has transformed to martensite. The contours show stresses at the wire surface ((a) and (b)), interior ((c) and (d)), and sample midplane ((e) and (f)). The images on the left ((a), (c), and (e)) show tensile stresses and the images on the right ((b), (d), and (f)) show the von Mises stresses. The scale bar on the left corresponds to the tensile stresses ((a), (c), and (e)) and the scale bar on the right corresponds to the von Mises stresses ((b), (d), and (f)).

boundary plane and that they are highest near the wire surface. In fact, the stresses relax very rapidly away from the grain boundary in the unconstrained regions.

In Fig. 10, we plot a typical result from one of the wires containing a triple junction, again with the contours showing stress values at the wire surface, interior, and midplane (containing the triple junction line). In (a) and (b), we see that surface stresses are highest around the triple junction line; in (c)–(f), we observe that the high stresses are not just confined to the surface—as was the case for the grain boundary—but rather are highly concentrated around the triple line.

The two examples shown match the expectation that the martensitic transformation results in large stress concentrations near grain boundaries. More importantly, they speak to the increased confinement around a triple junction as compared to a single grain boundary. The stress fields and amplitudes, however, naturally depend on grain orientation. After performing 40 similar simulations with randomized grain orientations, however, we find that the conclusions above hold

true in general. In Figs. 11(a) and 11(b), we show cumulative distributions of the maximum von Mises and rupture (perpendicular to grain boundary) stresses for different grain orientations. When evaluating absolute stress values, we integrate the output stresses over a characteristic area of grain boundary (5% of the wire cross section) to avoid capturing any numerical stress singularities at the wire surface.[46,47]

The large strains of the martensitic transformation combined with the purely elastic material model are observed to result in very high stresses in Fig. 11. Furthermore, the influence of grain misorientation is observed to be extremely high, with stress concentrations varying between zero and several gigapascals for different simulations; for comparison, the plastic yield stress of single crystalline austenitic Cu-Zn-Al is ~350 MPa.[62] Interestingly, the maximum distortional stresses near the triple junction are similar to those in the case of the grain boundary; shear stresses, due to expansion/contraction of the transforming grain, are high in both cases. The rupture stresses, however, are much higher at the triple
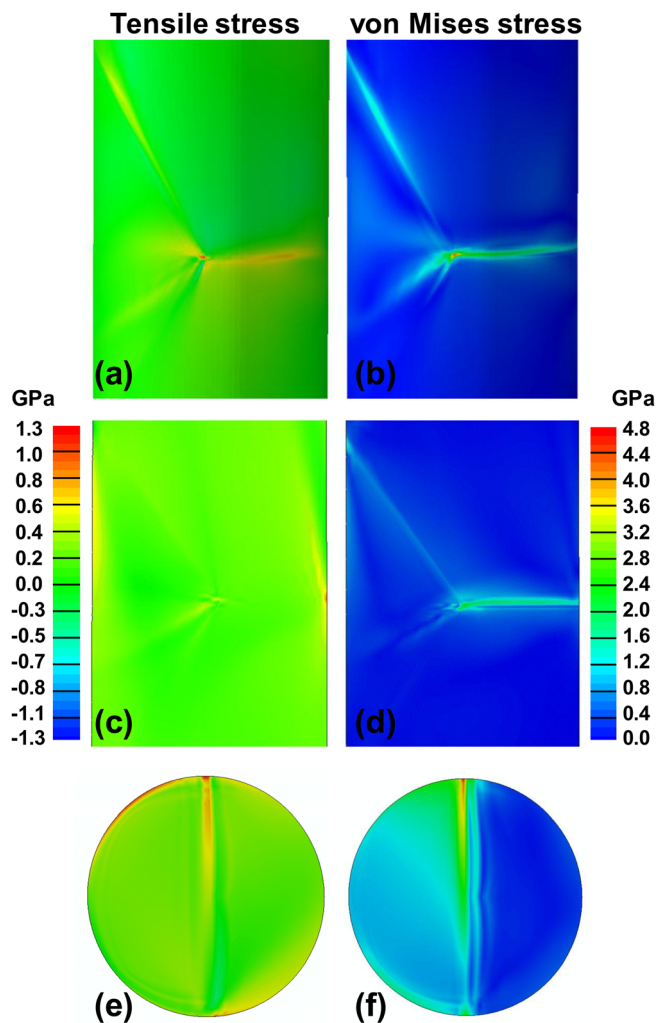

FIG. 10. Stresses near triple junction after the upper grain has transformed to martensite. The contours show stresses at the wire surface ((a) and (b)), interior ((c) and (d)), and sample midplane ((e) and (f)). The images on the left ((a), (c), and (e)) show tensile stresses and the images on the right ((b), (d), and (f)) show the von Mises stresses. The scale bar on the left corresponds to the tensile stresses ((a), (c), and (e)) and the scale bar on the right corresponds to the von Mises stresses ((b), (d), and (f)).
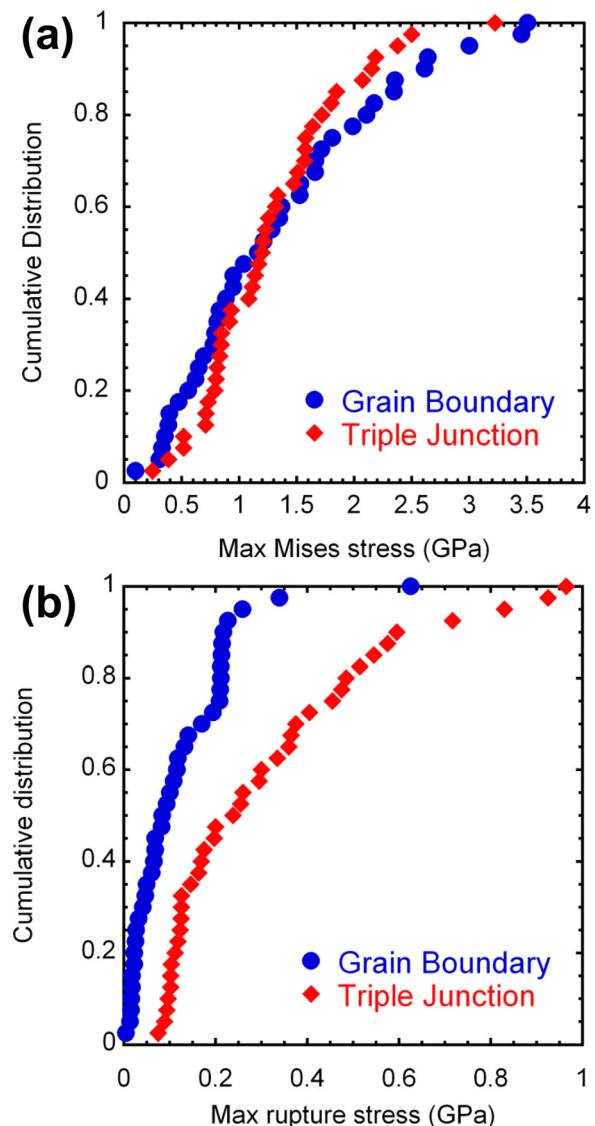

FIG. 11. Maximum (a) von Mises and (b) rupture stresses at grain boundary (blue circles) and triple junction (red diamonds) from 40 simulations with different random grain orientations.

junction than they are at the grain boundary. Interestingly, rupture stress is used in the fracture toughness failure criterion for polycrystalline Ni-Ti containing a crack[63] and is more likely the important one for control of SMA brittleness.

VI. CONCLUSIONS: THE ROLE OF GRAIN CONSTRAINT ON FRACTURE

The effect of grain constraint on the martensitic transformation in Cu-Zn-Al has been studied using *in situ* microscopy deformation experiments as well as finite element modeling. The results presented here speak of transformation-incompatibility stresses concentrated near grain boundaries and triple junctions, which affect the kinematics of the transformation. Such stress concentrations, together with the lack of a stress-relieving mechanism, have been put forward as an explanation for the brittleness of polycrystalline Cu-based SMAs. Towards the goal of designing high-performing SMAs that do not fracture—without incurring the cost and limitations of single crystal production—three conclusions can be made:

First, the morphology complexity near the triple junction is found to be higher than near simple grain boundaries; in particular, the nucleation of a second martensite variant from the triple junction is evidence of high stress concentrations. Finite element modeling also shows that transformation-induced rupture stresses are generally expected to be higher near a triple junction than near a simple grain boundary. This aligns with our previous study on superelasticity of Cu-Al-Ni, where we showed that wires with a near-bamboo microstructure fracture intergranularly at triple junctions.[18] We therefore conclude that triple junctions are the most detrimental microstructural feature to Cu-based SMAs. In order to avoid fracture and achieve good SMA properties, triple junctions should be avoided, and the bamboo structure is viewed as a preferred oligocrystalline form.

Second, the *in situ* experiments as well as the modeling revealed severe grain constraint near individual grain boundaries. This connects to our previous study where we showed that fatigue fracture in Cu-Zn-Al wires with a bamboo grain structure is intergranular.[19] On the other hand, the martensite morphology around grain boundaries is less complex than near the triple junction and the rupture stresses are estimated to be lower. Furthermore, our previous study demonstrated that wires with a bamboo grain structure can undergo multiple superelastic and thermal cycles to large strains. We therefore conclude that the total grain boundary area should be made as small as possible, but that a small area can be permitted while still avoiding fracture.

Third, the *in situ* experiments show that the phase transformation is sequential—not only with respect to grain orientation—but also with respect to different regions of the wire. Near grain boundaries, the transformation may only be partial as long as deformation can be accommodated in unconstrained, monocrystalline regions of the wire. Therefore, because the amount of transformation near grain boundaries can be very small as long as austenitic single crystal-like regions exist elsewhere, stresses may be significantly reduced. This is in contrast to conventional bulk polycrystals

where there are no "easy" regions and deformation necessarily must be accommodated near boundaries and triple junctions. We therefore conclude that a microstructure geometry designed to include unconstrained, "easily transforming," regions is preferable, because it reduces the amount of transformation needed near grain boundaries.

APPENDIX: TRANSFORMATION MATRICES

Transformation matrices for the cubic to monoclinic martensitic transformation in Cu-Zn-Al

$$U_1 = \begin{Bmatrix} \alpha & \delta & 0 \\ \delta & \beta & 0 \\ 0 & 0 & \gamma \end{Bmatrix} \quad U_2 = \begin{Bmatrix} \alpha & -\delta & 0 \\ -\delta & \beta & 0 \\ 0 & 0 & \gamma \end{Bmatrix}$$

$$U_3 = \begin{Bmatrix} \beta & \delta & 0 \\ \delta & \alpha & 0 \\ 0 & 0 & \gamma \end{Bmatrix} \quad U_4 = \begin{Bmatrix} \beta & -\delta & 0 \\ -\delta & \alpha & 0 \\ 0 & 0 & \gamma \end{Bmatrix}$$

$$U_5 = \begin{Bmatrix} \beta & 0 & \delta \\ 0 & \gamma & 0 \\ \delta & 0 & \alpha \end{Bmatrix} \quad U_6 = \begin{Bmatrix} \beta & 0 & -\delta \\ 0 & \gamma & 0 \\ -\delta & 0 & \alpha \end{Bmatrix}$$

$$U_7 = \begin{Bmatrix} \alpha & 0 & \delta \\ 0 & \gamma & 0 \\ \delta & 0 & \beta \end{Bmatrix} \quad U_8 = \begin{Bmatrix} \alpha & 0 & -\delta \\ 0 & \gamma & 0 \\ -\delta & 0 & \beta \end{Bmatrix}$$

$$U_9 = \begin{Bmatrix} \gamma & 0 & 0 \\ 0 & \alpha & \delta \\ 0 & \delta & \beta \end{Bmatrix} \quad U_{10} = \begin{Bmatrix} \gamma & 0 & 0 \\ 0 & \alpha & -\delta \\ 0 & -\delta & \beta \end{Bmatrix}$$

$$U_{11} = \begin{Bmatrix} \gamma & 0 & 0 \\ 0 & \beta & \delta \\ 0 & \delta & \alpha \end{Bmatrix} \quad U_{12} = \begin{Bmatrix} \gamma & 0 & 0 \\ 0 & \beta & -\delta \\ 0 & -\delta & \alpha \end{Bmatrix},$$

$\alpha = 1.0101$, $\beta = 1.0866$, $\delta = 0.0249$, and $\gamma = 0.9093$ (Ref. [56]).

The transformation strain matrices, E_i, are related to the transformation matrices, U_i, through the relation

$$\mathbf{E_i} = \mathbf{U_i} - \mathbf{I}. \tag{A1}$$

[1]K. Otsuka, C. M. Wayman, K. Nakai, H. Sakamoto, and K. Shimizu, Acta Metall. **24**, 207 (1976).
[2]T. Tadaki, K. Otsuka, and K. Shimizu, Ann. Rev. Mater. Sci. **18**, 25 (1988).
[3]C. M. Wayman, Prog. Mater. Sci. **36**, 203 (1992).
[4]H. Horikawa, S. Ichinose, K. Morii, S. Miyazaki, and K. Otsuka, Metall. Trans. A **19**, 915 (1988).
[5]J. Pfetzing-Micklich, C. Somsen, A. Dlouhy, C. Begau, A. Hartmaier, M. F. X. Wagner, and G. Eggeler, Acta Mater. **61**, 602 (2013).
[6]R. Araya, M. Marivil, C. Mir, O. Moroni, and A. Sepulveda, Mater. Sci. Eng. A **496**, 209 (2008).
[7]S. Montecinos, A. Cuniberti, and A. Sepulveda, Mater. Character. **59**, 117 (2008).

[8]Y. Sutou, T. Omori, K. Yamauchi, N. Ono, R. Kainuma, and K. Ishida, Acta Mater. **53**, 4121 (2005).

[9]A. Creuziger and W. C. Crone, Mater. Sci. Eng. A **498**, 404 (2008).

[10]S. Miyazaki, T. Kawai, and K. Otsuka, Scr. Metall. **16**, 431 (1982).

[11]Q. P. Sun and Y. J. He, Int. J. Solids Struct. **45**, 3868 (2008).

[12]S. Miyazaki and K. Otsuka, Isij Int. **29**, 353 (1989).

[13]S. Miyazaki, K. Otsuka, H. Sakamoto, and K. Shimizu, Trans. Jpn. Inst. Met. **22**, 244 (1981).

[14]H. Sakamoto, Y. Kijima, and K. Shimizu, Trans. Jpn. Inst. Met. **23**, 585 (1982).

[15]H. Sakamoto and K. Shimizu, Trans. Jpn. Inst. Met. **27**, 601 (1986).

[16]H. Sakamoto and K. Shimizu, Trans. Jpn. Inst. Met. **27**, 592 (1986).

[17]H. Sakamoto, K. Shimizu, and K. Otsuka, Trans. Jpn. Inst. Met. **22**, 579 (1981).

[18]S. M. Ueland, Y. Chen, and C. A. Schuh, Adv. Funct. Mater. **22**, 2094 (2012).

[19]S. M. Ueland and C. A. Schuh, Acta Mater. **60**, 282 (2012).

[20]Y. Chen, X. X. Zhang, D. C. Dunand, and C. A. Schuh, Appl. Phys. Lett. **95**, 171906 (2009).

[21]R. Delville, S. Kasinathan, Z. Y. Zhang, J. Van Humbeeck, R. D. James, and D. Schryvers, Philos. Mag. **90**, 177 (2010).

[22]R. Delville, D. Schryvers, Z. Y. Zhang, and R. D. James, Scr. Mater. **60**, 293 (2009).

[23]X. L. Meng, W. Cai, Y. D. Fu, J. X. Zhang, and L. C. Zhao, Acta Mater. **58**, 3751 (2010).

[24]S. Singh, R. K. Roy, M. Ghosh, A. Mitra, and A. K. Panda, J. Appl. Phys. **112**, 103512 (2012).

[25]Y. L. Liao, C. Ye, D. Lin, S. Suslov, and G. J. Cheng, J. Appl. Phys. **112**, 033515 (2012).

[26]V. Vega, L. Gonzalez, J. Garcia, W. O. Rosa, D. Serantes, V. M. Prida, G. Badini, R. Varga, J. J. Sunol, and B. Hernando, J. Appl. Phys. **112**, 033905 (2012).

[27]L. C. Brinson, I. Schmidt, and R. Lammering, J. Int. Mater. Syst. Struct. **13**, 761 (2002).

[28]L. C. Brinson, I. Schmidt, and R. Lammering, J. Mech. Phys. Solids **52**, 1549 (2004).

[29]S. Ichinose, Y. Funatsu, and K. Otsuka, Acta Metall. **33**, 1613 (1985).

[30]H. F. Tian, J. B. Lu, J. Ma, H. L. Shi, H. X. Yang, G. H. Wu, and J. Q. Li, J. Appl. Phys. **112**, 033904 (2012).

[31]T. Niendorf, J. Lackmann, B. Gorny, and H. J. Maier, Scr. Mater. **65**, 915 (2011).

[32]F. Auricchio and R. L. Taylor, Comput. Methods Appl. Mech. Eng. **143**, 175 (1997).

[33]F. Auricchio, R. L. Taylor, and J. Lubliner, Comput. Methods Appl. Mech. Eng. **146**, 281 (1997).

[34]L. C. Brinson and R. Lammering, Int. J. Solids Struct. **30**, 3261 (1993).

[35]D. Grandi, M. Maraldi, and L. Molari, Acta Mater. **60**, 179 (2012).

[36]V. I. Levitas and M. Javanbakht, Int. J. Mater. Res. **102**, 652 (2011).

[37]P. Thamburaja and L. Anand, J. Mech. Phys. Solids **49**, 709 (2001).

[38]L. Qiao, J. J. Rimoli, Y. Chen, C. A. Schuh, and R. Radovitzky, Phys. Rev. Lett. **106**, 085504 (2011).

[39]Y. G. Cui, J. F. Wan, J. H. Zhang, and Y. H. Rong, J. Appl. Phys. **112**, 094908 (2012).

[40]K. Gall, T. J. Lim, D. L. McDowell, H. Sehitoglu, and Y. I. Chumlyakov, Int. J. Plast. **16**, 1189 (2000).

[41]T. Waitz, T. Antretter, F. D. Fischer, N. K. Simha, and H. P. Karnthaler, J. Mech. Phys. Solids **55**, 419 (2007).

[42]W. M. Lee and M. A. Zikry, Mater. Sci. Eng. A **535**, 264 (2012).

[43]T. Y. Kim, J. E. Dolbow, and E. Fried, Int. J. Solids Struct. **49**, 3942 (2012).

[44]A. K. Kanjarla, P. Van Houtte, and L. Delannay, Int. J. Plast. **26**, 1220 (2010).

[45]S. Li, J. Q. Zhou, L. Ma, N. Xu, R. T. Zhu, and X. H. He, Comput. Mater. Sci. **45**, 390 (2009).

[46]A. Y. Kuo, J. Appl. Mech. **56**, 585 (1989).

[47]D. Munz and Y. Y. Yang, J. Appl. Mech. **59**, 857 (1992).

[48]S. N. Luo, T. C. Germann, T. G. Desai, D. L. Tonks, and Q. An, J. Appl. Phys. **107**, 123507 (2010).

[49]X. Balandraud and G. Zanzotto, J. Mech. Phys. Solids **55**, 194 (2007).

[50]C. S. Hau-Riege and C. V. Thompson, Appl. Phys. Lett. **77**, 352 (2000).

[51]D. T. Walton, H. J. Frost, and C. V. Thompson, Appl. Phys. Lett. **61**, 40 (1992).

[52]See supplementary material at http://dx.doi.org/10.1063/1.4817170 for original (unprocessed) micrographs used in this work.

[53]S. M. Ueland and C. A. Schuh, "Transition from many domain to single domain martensite morphology in small-scale shape memory alloys," Acta Mater. (published online).

[54]R. Stalmans, J. Vanhumbeeck, and L. Delaey, Acta Metall. Mater. **40**, 2921 (1992).

[55]J. F. Luo, S. C. Mao, X. D. Han, Z. Zhang, J. Wu, and M. H. Wub, J. Appl. Phys. **102**, 043526 (2007).

[56]K. Bhattacharya, *Microstructure of Martensite: Why It Forms and How It Gives Rise to the Shape-Memory Effect* (Oxford University Press, Oxford, 2003).

[57]P. L. Rodriguez, F. C. Lovey, G. Guenin, J. L. Pelegrina, M. Sade, and M. Morin, Acta Metall. Mater. **41**, 3307 (1993).

[58]P. Sittner and V. Novak, Int. J. Plast. **16**, 1243 (2000).

[59]B. Verlinden, T. Suzuki, L. Delaey, and G. Guenin, Scr. Metall. **18**, 975 (1984).

[60]S. Chakravorty and C. M. Wayman, Acta Metall. **25**, 989 (1977).

[61]Z. Yosibash, A. Bussiba, and I. Gilad, Int. J. Fract. **125**, 307 (2004).

[62]J. R. Davis, *ASM Speciality Handbook—Copper and Copper Alloys* (ASM International, 2001).

[63]S. Daly, A. Miller, G. Ravichandran, and K. Bhattacharya, Acta Mater. **55**, 6322 (2007).